

High-temperature phase transitions and low-temperature magnetic ordering in SrRuO₃ and CaRuO₃ ceramics studied using perturbed-angular-correlation spectroscopy

Gary L. Catchen and Todd M. Rearick

*Department of Nuclear Engineering and Electronic Materials and Processing Research Laboratory,
The Pennsylvania State University, University Park, Pennsylvania 16802*

Darrell G. Schlom

Department of Materials Science and Engineering, The Pennsylvania State University, University Park, Pennsylvania 16802

(Received 1 July 1993; revised manuscript received 17 August 1993)

Perturbed-angular-correlation (PAC) spectroscopy was used to measure nuclear-electric-quadrupole interactions in the orthorhombically-distorted perovskites SrRuO₃ and CaRuO₃ over temperatures ranging from laboratory to very high temperatures. At 77 K, PAC spectroscopy was used to measure combined electric-quadrupole and magnetic-dipole interactions in magnetically ordered SrRuO₃ and pure electric-quadrupole interactions in paramagnetic CaRuO₃. The ¹¹¹In→¹¹¹Cd PAC probe was used for these measurements, and it substituted into the Ru site in SrRuO₃ and very likely into the Ru site in CaRuO₃. The temperature dependence of the electric-field-gradient (EFG) parameters for SrRuO₃ indicates the onset of a structural phase transition at approximately 800 K. The presence of this transition indicates that the laboratory-temperature structure of SrRuO₃ has lower-than-cubic symmetry. At very high temperatures > 1600 K, the structure of CaRuO₃, as given by the EFG parameters, becomes very similar to the laboratory-temperature structure of SrRuO₃. At 77 K in SrRuO₃, the measured Ru-site supertransferred hyperfine field is 39±3 kOe. Using ⁹⁹Ru and ⁵⁷Fe Mössbauer-effect information and other ¹¹¹In→¹¹¹Cd PAC measurements, the magnetic hyperfine fields at the Ru site in SrRuO₃ and at the Fe site in PrFeO₃ are compared.

I. INTRODUCTION

Strontium ruthenium oxide SrRuO₃ (SR) and calcium ruthenium oxide CaRuO₃ (CR) have perovskite crystal structures and metallic electrical conductivity.¹⁻¹³ These properties make SR and CR important candidate materials for forming epitaxial heterostructures with other perovskites when layers that have metallic conductivity are desired, e.g., electrodes for superconductor-normal-metal-superconductor junctions,⁹⁻¹¹ electrodes for field-effect-transistor structures that have oxide-superconductor channels,¹² and electrodes for ferroelectrics.^{8,13}

Even though the SR and CR compounds have been known for well over 30 years, agreement on the crystal structures is not to be found,^{1,4,5,7} and the magnetic properties are not well understood.^{2,3,14,15} Reports of the earlier crystal-structure investigations indicate that both SR and CR are orthorhombically-distorted perovskites that have the GdFeO₃ structure and the space group *Pbnm* (*D*_{2h}¹⁶).^{1,4} Whereas, several more recent investigations produced conflicting reports in which SR is assigned a cubic lattice⁵ and space group⁷ and CR is assigned a different orthorhombic space group.⁷ Similarly, the results of diffraction studies on single-crystal thin films are consistent with SR having orthorhombic crystal symmetry.⁸

Initial macroscopic magnetic-susceptibility measurements performed by Callaghan, Moeller, and Ward² on ceramic samples of SR and CR show that both com-

pounds follow a Curie-Weiss law at high temperatures. On SR, these measurements show the onset of ferromagnetism at 160±10 K.² They estimate the saturation magnetization to be 0.85 μ_B per Ru atom,² (in which μ_B is the Bohr magneton). On CR, these measurements, which were made down to 77 K, show no effects of magnetic ordering. However, on CR, Longo, Raccach, and Goodenough³ performed magnetic-susceptibility measurements down to 4.2 K, and they performed bulk magnetization measurements at 4.2 K, in which they found evidence for parasitic ferromagnetism. From these results, they concluded that CR is antiferromagnetic below a Néel temperature of 110±10 K.³ On SR, they performed neutron diffraction and derived a ferromagnetic component μ=1.4±0.4 μ_B per Ru atom.³ In addition, they reported high-field magnetization measurements on SR that gave a ferromagnetic component μ=1.55μ_B per Ru atom at 125 kOe and 4.2 K, which did not appear to be saturated.³ Subsequently, Gibb and co-workers^{14,15} performed low-temperature (77 and 4.2 K) ⁹⁹Ru Mössbauer-effect (ME) spectroscopy on SR and CR powder absorbers. Their results show that in SR the ⁹⁹Ru nucleus undergoes a strong magnetic hyperfine interaction (MHI) at both 77 and 4.2 K (Ref. 14) and that in CR the ⁹⁹Ru nucleus does not undergo a measurable MHI.¹⁵ These results unambiguously indicate that above 4.2 K SR is magnetically ordered and CR is not. Thus the initial report³ of antiferromagnetism in CR is incorrect.

Both the high-temperature crystal structures of SR and CR and the low-temperature magnetic properties, pri-

marily of SR, involve vagaries. Specifically, as powder x-ray diffraction indicates, the CR perovskite crystal is sufficiently distorted that representing it by orthorhombic symmetry does not appear likely to be in error. But, because similar measurements on the SR crystal show very little distortion from cubicity, the symmetry of the SR structure is difficult to determine and therefore remains in question. In the conventional description of SR and CR, in which a Ru^{4+} ion is located at the center of an octahedral crystal field of O^{2-} ions, the Ru^{4+} electrons have low-spin $(t_{2g})^4(e_g)^0$ configurations. When no orbital angular momentum contributes to the d -electron magnetic moment, we expect to observe the spin-only value of the saturation magnetization $M_s = g\mu_B S$, in which, for low-spin d^4 , $S=1$ and $M_s = 2\mu_B$.^{2,3} The various measurements on ferromagnetic SR gave M_s values that are significantly less than $2\mu_B$. Because SR has metallic electrical conductivity, the complementary explanation of the low M_s values that others have offered^{2,3} is that in SR some of the d -electrons are delocalized in energy bands.^{2,3} In this situation, itinerant exchange would contribute to the magnetic ordering along with superexchange through Ru-O-Ru bonds, which is the primary magnetic-ordering mechanism in magnetic perovskites. Similarly, the magnetic hyperfine field (MHF) measured by ^{99}Ru ME spectroscopy can be accounted for by the field that one $4d$ electron would generate at the Ru nucleus via core polarization.¹⁵ Although these explanations describe the magnetic phenomena, they are far from complete. Thus the description of both the high-temperature crystal structures and the low-temperature magnetic properties of SR and CR appear to be incomplete if not incorrect. To seek new information about both of these aspects of the SR and CR properties, we have performed a series of perturbed-angular-correlation (PAC) measurements on SR and CR using the $^{111}\text{In} \rightarrow ^{111}\text{Cd}$ probe. To interpret these measurements, we use our experience with and information obtained from PAC measurements performed on other ABO_3 perovskites.¹⁷⁻¹⁹

The SR and CR compounds have structures that are very similar to those of the rare-earth orthoferrites (REO's) $R\text{FeO}_3$ ($R = \text{La}, \text{Pr}, \dots, \text{Lu}$ and Y), namely, the orthorhombic GdFeO_3 structure, although for SR the specific space group is in question.¹⁶ Unlike SR and CR, the REO's are electrical insulators, and the Fe^{3+} d electrons have high-spin $(t_{2g})^3(e_g)^2$ configurations. Also, the REO's are canted antiferromagnets that have high transition temperatures. Recently we have reported an extensive PAC study of combined magnetic-dipole and electric-quadrupole hyperfine interactions in the REO's in which we used the $^{111}\text{In} \rightarrow ^{111}\text{Cd}$ probe.¹⁷ With regard to the present study, the specific quantities of the structurally similar REO's that may be useful are the Fe-site supertransferred hyperfine fields (STHF's) measured by PAC spectroscopy and the total MHF's measured by ^{57}Fe ME spectroscopy. Because the members of the REO family have very similar structural and magnetic properties, they form a series of "model systems" as the rare-earth atoms vary from La to Lu. The structure of SR is very similar to the PrFeO_3 structure. For this reason, we

may infer information about the magnetic properties of SR, by comparing the Ru-site STHF measured by PAC spectroscopy and the total MHF measured by ^{99}Ru ME spectroscopy to those quantities measured at the Fe site for this REO model system. Specifically, we may be able to more precisely determine the role of itinerant exchange in the magnetic ordering of SR. In a similar approach, we can compare the electric-field-gradient (EFG) parameters, V_{zz} , η , and δ measured at the Ru sites in SR and CR to those measured at the B sites in other ABO_3 perovskites such as BaTiO_3 that undergo structural phase transitions.^{18,20} The specific purpose of this comparison is to resolve subtleties in the crystal structures of SR and CR.

II. EXPERIMENTAL DETAILS

Ceramic samples of SrRuO_3 and CaRuO_3 were prepared by (1) mixing accurately weighed powders of Ru metal and either SrCO_3 and CaCO_3 (2) adding several microcuries of ^{111}In activity to the powder mixture via a small amount of a dilute HCl solution that contained the carrier-free radioactivity, (3) drying the mixture in a furnace, and (4) pressing several small pellets (0.5–1 g) and sintering them in air in a tube furnace. The sintering temperatures ranged from 1500 to 1800 K. To check the phase purity of the radioactive samples, x-ray-diffraction patterns were measured on small amounts of powder taken from the samples on which PAC measurements were made. For the most part, the samples were composed primarily of a single perovskite phase. However, the patterns usually showed several low-intensity lines that did not represent the perovskite phases. We attributed these lines to small amounts of contaminant phases, which comprised not more than several percent of the sample. Figure 1 presents two diffraction patterns that are representative of those obtained for SR and CR. The presence of the contaminant phases did not correlate strongly with the sintering temperature.

A recent review²¹ presents most of the experimental details involved with performing and analyzing the PAC experiments. Some of the experimental time distributions were collected using a four-CsF-detector PAC spectrometer, which has a time resolution of ≈ 1 nsec, full width at half maximum (FWHM), and the others were collected using a four-BaF₂-detector PAC spectrometer, which has a time resolution of ≈ 800 psec FWHM. Both spectrometers collect four (two 90° and two 180°) coincidences concurrently. The experimental perturbation functions $A_{22}G_{22}(t_i)$ were obtained from the measured correlation functions, i.e., time distributions, $W_{jk}(\theta_{jk}, t_i)$ that represent the primary experimental data (the subscripts j and k refer to the coincidence between the respective detectors, and i refers to the time interval). Specifically, the ratio method was used to obtain $A_{22}G_{22}(t_i)$ from the four measured correlation functions.¹⁶ Simple tube furnaces were used to maintain the elevated temperatures during the PAC measurements performed below ≈ 1300 K. For those performed at higher temperatures, a specifically designed furnace was used.²² The furnaces

were controlled to ± 1 K. For the measurements performed at 77 K, a simple liquid-nitrogen-filled Dewar was used to maintain the sample temperature.

To analyze the perturbation functions that did not con-

$$-A_{22}G_{22}(t_i) = A_1 \left[S_0(\eta_1) + \sum_{k=1}^3 S_k(\eta_1) \exp(-\delta_1 \omega_k t_i) \cos(\omega_k t_i) \right] + A_2 \left[S_0(\eta_2) + \sum_{k=4}^6 S_k(\eta_2) \exp(-\delta_2 \omega_k t_i) \cos(\omega_k t_i) \right] + A_3. \quad (1)$$

Here A_1 and A_2 are the normalization factors, δ_1 and δ_2 are the line-shape parameters, which give the relative widths of Lorentzian frequency distributions (of the corresponding sets of ω_k 's) that give rise to static line-broadening, and A_3 takes into account the effects of γ -rays that the sample absorbs and the effects of the probe atoms that are not in well-defined chemical environments, namely, either site one or site two. The frequencies ω_k and the $S_k(\eta)$ coefficients describe a static interaction in a polycrystalline source.²¹ Equation (1) was fitted to the perturbation functions. Generally, the one-site model (to which a zero-frequency term A_3 was sometimes added) provided accurate fits to the CR perturbation functions. For SR, usually the two-site model (to which A_3 was sometimes added) provided accurate fits.

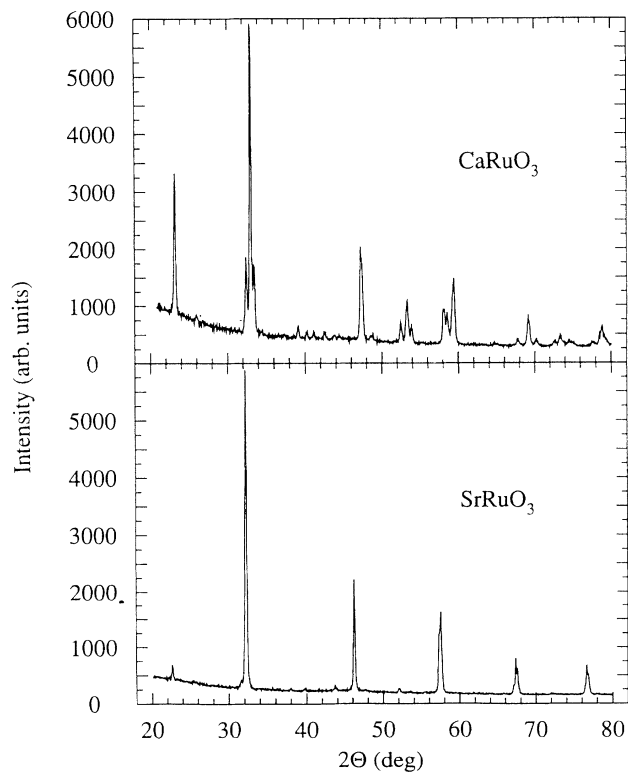


FIG. 1. X-ray powder-diffraction patterns for SrRuO₃ (lower) and CaRuO₃ (upper) ¹¹¹In-doped ceramic samples. The measured patterns show good agreement with the reference lines. However, some small peaks that represent contaminant phases are evident.

tain the effects of magnetic-dipole interactions, we used either a one-site ($A_2=0$) or a two-site model for nuclear electric-quadrupole interactions in a polycrystalline source:

The free parameters for site one ($A_1, \delta_1, \omega_1, \omega_2$) and those for site two ($A_2, \delta_2, \omega_4, \omega_5$) when applicable were derived from the fits. For each site, the ratios ω_2/ω_1 and ω_5/ω_4 were used to determine the corresponding quadrupole frequencies ω_Q and asymmetry parameters η . The non-vanishing EFG components V_{ii} in the principal-axis system where the probe nucleus is at the origin are related to the quadrupole frequency ω_Q and the asymmetry parameter η by $\omega_Q = [eQV_{zz}/4I(2I-1)\hbar]$ and $\eta = (V_{xx} - V_{yy})/V_{zz}$, in which Q is the nuclear quadrupole moment (0.77 b) of the spin $I = \frac{5}{2}$ intermediate nuclear level in the ¹¹¹Cd probe nucleus. The site-occupancy fractions are given by $f_i = A_i / (A_1 + A_2 + A_3)$, $i = 1, 2, 3$.

To analyze perturbation functions that showed the effects of both magnetic-dipole and electric-quadrupole interactions, we used the methods that Ref. 17 describes in detail. Specifically, for SR measured at 77 K, we have the situation in which $y = (\omega_L/\omega_Q) \gg 1$, and ω_L is the Larmor frequency. For this situation, the interaction frequencies can be determined by fitting the perturbation functions to

$$-A_{22}G_{22}(t_i) = S_0 + \sum_{k=1}^n S_k \exp[-\frac{1}{2}(\delta \omega_k t_i)^2] \cos(\omega_k t_i), \quad (2)$$

in which n is the total number of frequencies. This model uses a single Gaussian line-shape factor. In the fitting process, the S_k coefficients, the line-shape parameters δ , and the frequencies ω_k were treated as free parameters and no sum constraints were used.

III. RESULTS

Figure 2 presents some perturbation functions and the corresponding Fourier transforms for a sample of SR measured at 290 K and 77 K. In the transform of the 290-K perturbation function, the peaks represent two sets of frequencies that correspond to two electric-quadrupole interactions. The major interaction indicated by ω_1 , ω_2 , and ω_3 involved approximately 88% of the probes. The primary frequency of the interaction $\omega_1 \approx 20$ Mrad sec⁻¹. The other interaction is not readily identified in the transform. In the transform of the 77-K perturbation function, a large peak at ≈ 20 Mrad sec⁻¹ is essentially absent. Instead, most if not all of the frequencies shown in this transform are shifted to much higher values. This shift of frequencies that occurs when the temperature is reduced below T_c (≈ 160 K) characterizes the presence of

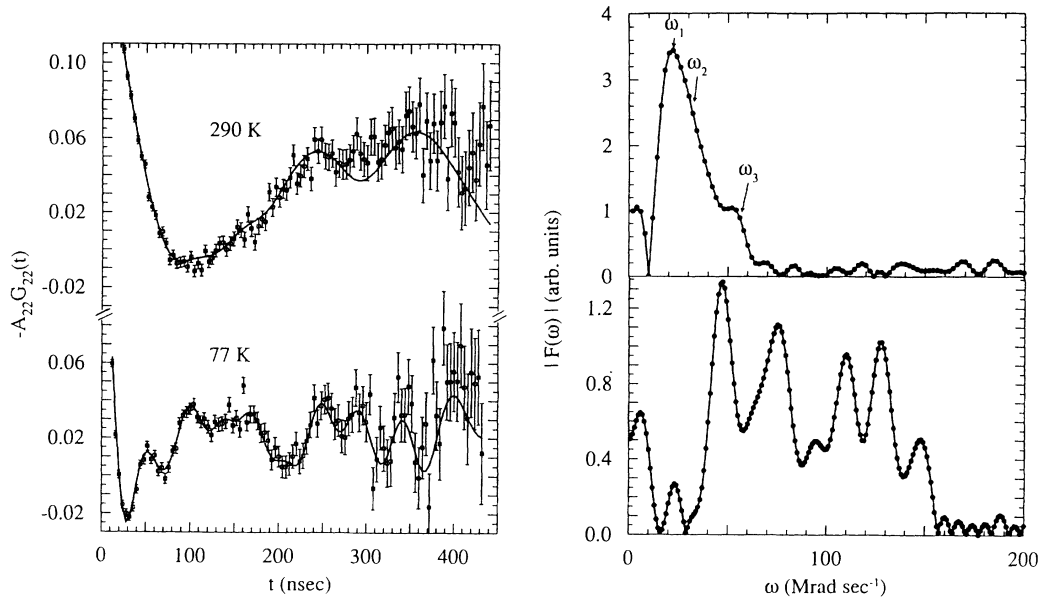


FIG. 2. Perturbation functions and Fourier transforms for a sample of SrRuO_3 measured at the indicated temperatures. For the 290-K perturbation function, the solid line represents a fit of Eq. (1) to the data. For the 77-K perturbation function the solid line represents a fit of Eq. (2) to the data.

a strong MHF ($\gamma \gg 1$) at the probe site. From our experience with the REO's, specifically PrFeO_3 ,¹⁷ we know that the substitution of the probe into the Fe site has associated with it this type of frequency shift when $T < T_N$.²³ Because the 77-K ^{99}Ru ME results^{14,15} on SR show the presence of a strong Ru-site MHF at this temperature, we expect the $^{111}\text{In} \rightarrow ^{111}\text{Cd}$ probe to undergo a large magnetic-dipole interaction in SR, if it were to substitute into the Ru site. Thus, the electric quadrupole interaction represented by the frequency set ω_1 , ω_2 , and ω_3 must have occurred at the Ru site in SR. Thus, in SR, the $^{111}\text{In} \rightarrow ^{111}\text{Cd}$ probe substitutes primarily into the Ru site. In Fig. 2, the second interaction involved $\approx 12\%$ of the probes. Because the second interaction involved a relatively small fraction of the probes, it is difficult to characterize. The presence of small amounts of contaminant phases in the samples where some of the probes could have substituted precludes assigning the second interaction either to the Sr site or elsewhere by default.

Figure 3 presents some perturbation functions for a sample of SR measured at elevated temperatures. For the perturbation functions measured below approximately 800 K, the frequencies shift to lower and lower values as temperature increases. At temperatures above 800 K, the perturbation functions show little temperature sensitivity, and they represent very weak interactions that show much static linebroadening. Figure 4 summarizes the EFG parameters for the primary interaction derived from fits to the SR perturbation functions. We fit most of the perturbation functions measured below 800 K using the two-site model, and we fit most of those measured at higher temperatures using the one-site model. For the temperature range from laboratory temperature to approximately 800 K, the values of V_{zz} decrease slowly as temperature increases. Near 800 K, the V_{zz} values de-

crease rapidly to relatively small values. Over the temperature range from laboratory temperature to approximately 800 K, the asymmetry parameter η remains relatively constant in value at about 0.5, and the line-shape parameter also remains relatively constant at very small values < 0.05 . Above ≈ 800 K, the η values become indeterminate, because the corresponding V_{zz} values are very small; and the δ values become very large. The site-occupancy fractions f also appear to change near 800 K. This change in f cannot be associated with a definite change in the second-site interaction, as the change could arise as an artifact of the fitting process. The error bars for the V_{zz} values near and above 800 K in Fig. 4 appear to be very large. These error bars are determined using standard nonlinear regression analysis. As such, they represent confidence intervals that reflect the uniqueness of the derived parameters. These large error bars do not mean that the V_{zz} values are indeterminate. They merely indicate that different sets of parameters could generate very similar fits to the corresponding perturbation functions. Although the fits to the higher-temperature perturbation functions are not unique, the derived parameters are self-consistent. That is, fits to similar-appearing perturbation functions, which are all of those measured above 800 K, yield V_{zz} values that have similar magnitudes.

Figure 5 presents some perturbation functions for samples of CR. For the perturbation functions measured from 77 K to approximately 1000 K, the frequencies and the asymmetries change very slowly. At the highest temperatures, the perturbation functions show a decrease in asymmetry; until, finally, those measured near 1600 K appear to be very similar to those measured on samples of SR at low temperatures, e.g., laboratory temperature. Figure 6 summarizes the EFG parameters derived from

fits to the CR perturbation functions. Most of the CR perturbation functions could be accurately represented using the one-site model. Over the entire temperature range, the V_{zz} -values slowly decrease as the temperature increases. Over the entire temperature range, the V_{zz} -values slowly decrease as the temperature increases. The line-shape parameter δ remains essentially constant. The site-occupancy fraction f remains essentially constant except at the higher temperature. Since these higher temperatures correspond to typical sintering temperatures, these variations in the site-occupancy fraction could simply reflect any of a myriad of possible thermally activated processes that occur at high temperatures. The temperature dependence of the asymmetry parameter η goes through a slight maximum near 800 K, and near 1000 K, it decreases rapidly to values for $T > 1600$ K that are similar to those measured on SR at laboratory temperature. The corresponding V_{zz} values for $T > 1600$ K are also similar to those measured on SR at laboratory temperature.

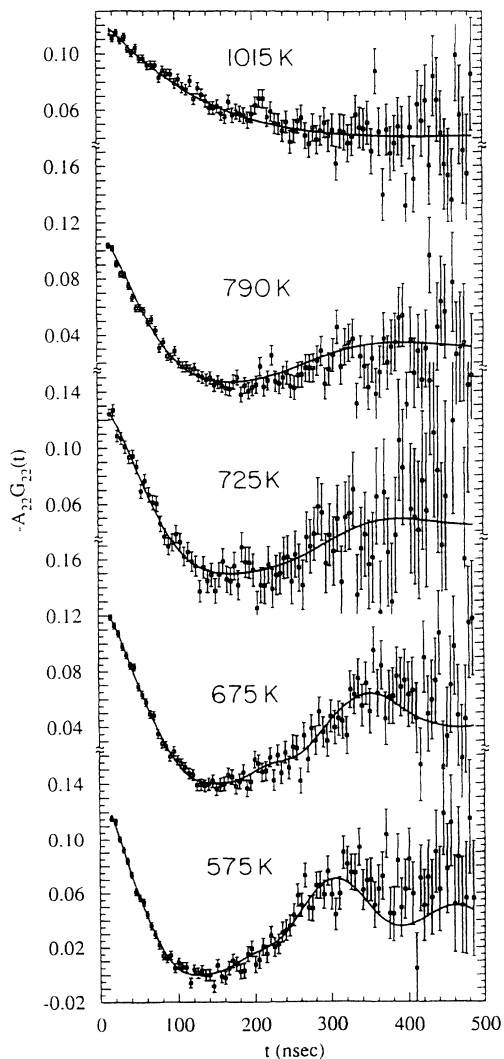


FIG. 3. Perturbation functions for SrRuO₃ measured at the indicated temperatures. The solid lines represent fits of Eq. (1) to the data.

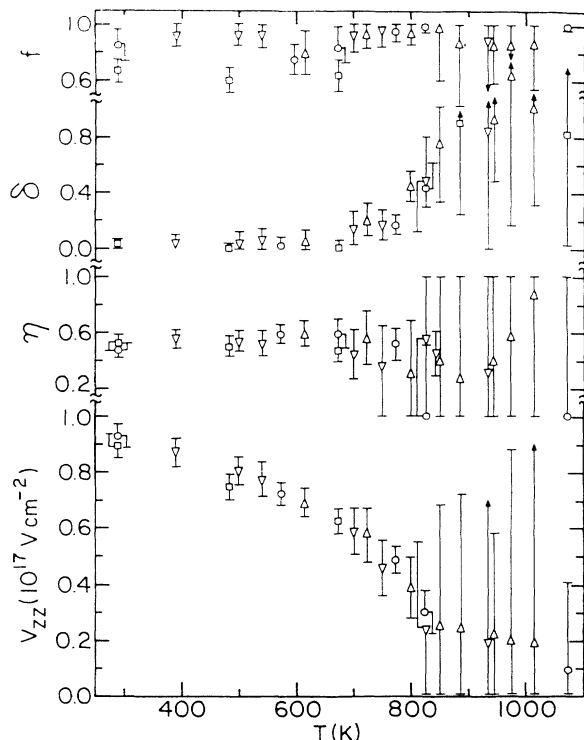


FIG. 4. Electric-field-gradient parameters measured over a large temperature range are presented for several samples of SrRuO₃. These parameters characterize the Ru-site interactions. The different symbols correspond to measurements on different samples.

The 77-K and 290-K perturbation functions are very similar. This result indicates that the probes do not undergo a measurable MHI at 77 K. Because the ⁹⁹Ru ME measurements¹⁵ indicate that CR is not magnetically ordered at 77 K, we cannot use the presence of a strong MHF at the probe site to assign the probe-site substitution. Instead, we compare the magnitudes and asymmetries of the rare-earth-site and Fe-site EFG's for $T > T_N$ in the REO's with the corresponding quantities for CR. At the rare-earth sites in REO's at 800 K, V_{zz} ranges from 7.5×10^{17} V cm⁻² for PrFeO₃ to 8.2×10^{17} V cm⁻² for LuFeO₃, and η is approximately 0.4 for PrFeO₃ and η decreases monotonically to near zero for LuFeO₃. At the Fe sites, V_{zz} ranges from 1×10^{17} V cm⁻² to 2×10^{17} V cm⁻² and η ranges from approximately 0.4 to 0.8. Thus, the lower-temperature V_{zz} and η values for CR more closely resemble the corresponding Fe-site values for V_{zz} and η for the REO's. This comparison is reasonable because CR and the REO's have similar structures and lattice parameters. In the absence of conflicting information, this comparison suggests that the ¹¹¹In → ¹¹¹Cd probe substitutes primarily into the Ru site in CR. Additionally, if the probe were not to substitute exclusively into the Ru site in CR, we would expect the probe to partition between the Ca site and the Ru site, because the Ru sites in both structures are similar in size and we know that the probe occupies the Ru-site in SR. We observe, however, essentially exclusive substitution of

the probe into one well-defined site in CR. Although these arguments are not conclusive, they suggest that the substitution of the $^{111}\text{In} \rightarrow ^{111}\text{Cd}$ probe into the Ru site in CR is highly likely.

IV. DISCUSSION

A. High-temperature phase transitions in SR and CR

Because the formal charge of the $^{111}\text{In}^{3+}$ probe ion differs from the native Ru^{4+} -ion charge, the probe ion could trap O vacancies. Consequently, trapped O vacancies could generate large EFG's at the probe site, which would not reflect either the strength or the symmetry of the probe-site crystal field. However, the measured temperature dependences of the Ru-site EFG parameters in either SR or CR do not show evidence for the thermally

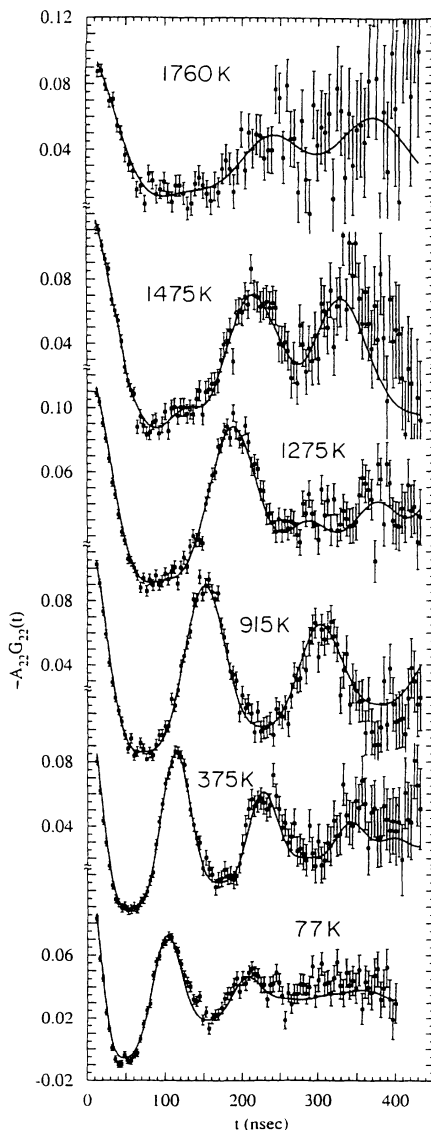


FIG. 5. Perturbation functions for CaRuO_3 samples measured at the indicated temperatures. The solid lines represent fits in Eq. (1) to the data.

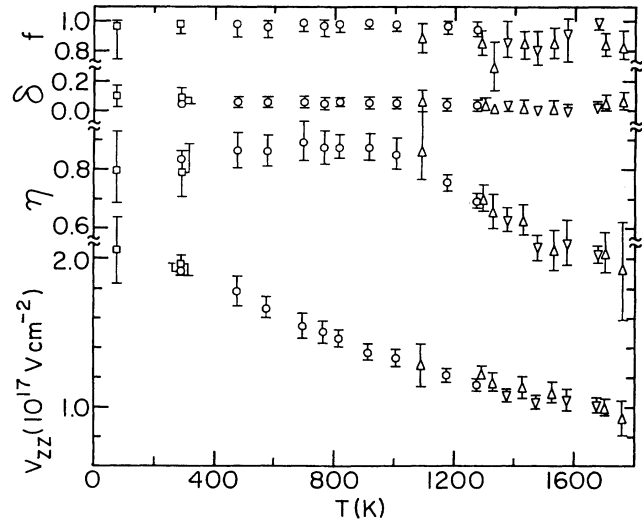


FIG. 6. Electric-field-gradient parameters measured over a large temperature range are presented for several samples of CaRuO_3 . The different symbols correspond to measurements on different samples.

activated detrapping of these defects. Furthermore, $^{111}\text{In} \rightarrow ^{111}\text{Cd}$ PAC measurements on the isostructural REO's show Fe-site EFG's that are very similar to those measured at the Ru sites in SR and CR. No formal charge difference exists between the $^{111}\text{In}^{3+}$ probe ion and the native Fe^{3+} ion in the REO's. For these reasons, we rule out the possibility that the Ru-site EFG's in SR and CR could be generated primarily by trapped O vacancies.

At the Ru site in SR, the laboratory-temperature EFG asymmetry is rather large $\eta \approx 0.5$, even though the SR crystal has near-tetragonal (or, perhaps, near-cubic) symmetry. Specifically the orthorhombic ($Pbmn$) space-group lattice parameters are $a = 5.5319(6)$ Å, $b = 5.5724(6)$ Å, and $c = 7.8496(15)$ Å.⁴ Thus the distortion in the Ru O-octahedra in SR is insufficient to account for this large asymmetry. Furthermore, from laboratory temperature to ≈ 800 K, the η temperature dependence is essentially constant. Over this temperature range, the EFG component V_{zz} decreases monotonically. The effect of increasing temperature is to reduce the strength of the Ru-site EFG, but not to change its asymmetry. The EFG asymmetry does not appear to arise from temperature-dependent effects of directional bonding, i.e., from either distortion of the Ru O octahedra or tilting of the octahedra with respect to each other. Similarly, the large asymmetry-parameter values suggest that the EFG principal axes at the Ru site are not aligned with the crystallographic axes. A possible explanation of the origins of this EFG asymmetry may lie in the details of the metal-oxygen bonding. Electron orbitals that are occupied but do not engage in σ -directional bonding could generate large asymmetries. Currently, we do not have access to theoretical methods that could be used to test this hypothesis.

The temperature dependences of the EFG parameters

V_{zz} , η , and δ for the Ru-site in SR indicate that the crystal undergoes a structural phase transition at approximately 800 K. From laboratory temperature to temperatures near 800 K, V_{zz} decreases, η remains relatively constant at ≈ 0.5 , and δ remains relatively small and constant at ≈ 0.05 . In the vicinity of 800 K, V_{zz} decreases abruptly to very small values near $0.1 \times 10^{17} \text{ V cm}^{-2}$ to $0.25 \times 10^{17} \text{ V cm}^{-2}$, η becomes indeterminate, and δ rapidly increases to large and uncertain values. As we mentioned above, the large errors associated with the data points in Fig. 4 measured near and above 800 K arise from the fitting process and reflect the lack of uniqueness of the parameters. Moreover, direct visual inspection of the shapes of the perturbation functions measured above 800 K indicates that they do not change shape appreciably, whereas, those measured below 800 K do change shape. Thus, the large errors associated with the parameters measured near and above 800 K do not prevent us from concluding that a phase transition does occur in SR near 800 K.

These temperature dependences of V_{zz} , η , and δ are qualitatively very similar to the corresponding temperature dependences at temperatures near the tetragonal-to-cubic transitions in the ferroelectric perovskites BaTiO_3 and KNbO_3 (measured by $^{181}\text{Hf} \rightarrow ^{181}\text{Ta}$ PAC).²⁰ This similarity in these temperature dependences suggests that, at temperatures above ≈ 800 K, the SR crystal structure has cubic symmetry. This condition implies that, below this temperature, the SR structure has lower-than-cubic, most likely, orthorhombic symmetry. In addition, the laboratory-temperature x-ray-diffraction studies that give cubic structures may be incorrect. Moreover, the lower-symmetry phases of BaTiO_3 and KNbO_3 are ferroelectric. In the case of SR, the proposed space group $Pbnm$ has a center of symmetry, which would preclude ferroelectricity. It is possible that a closely related, noncentrosymmetric space group may actually be the correct representation and that SR may be ferroelectric. This possibility would explain the remarkable similarity between the temperature dependences of the EFG parameters for SR and the ferroelectrics BaTiO_3 and KNbO_3 .

Over a large range of elevated temperature, $T < 1000$ K, the EFG at (most likely) the Ru site in CR has a very large asymmetry $\eta \approx 0.8$. At laboratory temperature, for CR, V_{zz} is approximately twice the corresponding value for SR. The CR perovskite structure, over this elevated temperature range, can be described as an array of tilted O octahedra.⁷ Above 1000 K, η decreases as temperature increases to a value of ≈ 0.5 at $T \approx 1700$ K, and V_{zz} decreases to a value of $\approx 1 \times 10^{17} \text{ V cm}^{-2}$. As the shapes of the 1760-K perturbation function in Fig. 5 and the 290-K perturbation function in Fig. 2 show, the high-temperature values of η and V_{zz} for CR are approximately the same as the corresponding laboratory-temperature values for SR. Thus, the high-temperature structure of CR is approximately the same as the low-temperature structure of SR. In this context, we can describe the CR structure as evolving from an array of tilted O octahedra at lower temperatures to an array of nontilted O octahedra at higher temperatures. The CR structure ap-

proaches the structure of SR in which the EFG asymmetry is nonvanishing $\eta \approx 0.5$. These results suggest that the high-temperature EFG asymmetry in CR and the low-temperature EFG asymmetry in SR have common origins.

B. Low-temperature magnetic hyperfine fields in SR

For SR, the 77-K perturbation functions and the associated Fourier transforms show the effects of a combined magnetic-dipole and electric-quadrupole interaction. Using Eq. (2), we were able to obtain fits that are good representations of the perturbation functions. The fits involve ten frequency components, but not all of these components necessarily correspond to the Ru-site combined interaction. As a result, we could only obtain the Larmor frequency reliably by averaging groups of frequencies. We could not obtain other information such as the angle between the magnetic-hyperfine-field direction and the EFG z-axis, which, in principle, can be discerned from further analysis of the frequency components.¹⁷ Thus at 77 K, the Larmor frequency that describes the Ru-site magnetic-dipole interaction in SR is $\omega_L = 58 \pm 5 \text{ Mrad sec}^{-1}$; and, using $\omega_L = g\mu_N H / \hbar$ and $g = -0.306$, the associated magnetic-hyperfine-field magnitude is $H_{\text{PAC}} = 39 \pm 3 \text{ kOe}$. For the purpose of comparison, the relative interaction strengths are $y = [\omega_L(77 \text{ K}) / \omega_Q(290 \text{ K})] = 22 \pm 2$.

To analyze the Ru-site MHF's, we note that the MHF measured by ^{99}Ru ME spectroscopy is $315 \pm 15 \text{ kOe}$ at 77 K.¹⁵ Using the rationale that we presented in the recent study of combined interactions in the REO's,¹⁷ we recognize the PAC-measured MHF as the supertransferred hyperfine field (STHF) and the ME-measured MHF as the total magnetic hyperfine field at the Ru-site in SR. The lattice parameters of LaFeO_3 are closest in size to those of SR, and the parameters for PrFeO_3 are almost as close.²⁴ The 800-K η values for LaFeO_3 and PrFeO_3 are 0.8 and 0.4, respectively. Because the EFG asymmetry for PrFeO_3 better matches that for SR, we choose PrFeO_3 as the REO model compound. To make comparisons between SR and PrFeO_3 , we note that, at 77 K, the reduced temperature for SR is $t_r = 0.52$ (based on $T_c = 160 \text{ K}$).² The total MHF of PrFeO_3 at this t_r value, measured by ^{57}Fe ME spectroscopy, is 463 kOe (based on $T_N = 707 \text{ K}$).²⁴ Now in the REO's, $S = \frac{5}{2}$ for the high-spin d^5 electron configuration. Since the d electrons are for the most part localized, conventional practice is to take $M_s = 5\mu_B$ per Fe atom,²⁵ which gives the ratio of local magnetic moments $[M_s(\text{Ru}) / M_s(\text{Fe})] = \frac{2}{5}$. If the d electrons were localized in both Sr and PrFeO_3 , as a crude approximation, we would expect both the total MHF and the STHF at the Ru site in SR to be reduced by a factor of $\frac{2}{5}$ from those quantities in PrFeO_3 . The ratio H_{STHF} / H should be the same for both compounds. For SR, $[H_{\text{STHF}}(\text{Cd}) / H(\text{Ru})] = 0.12 \pm 0.01$; and for PrFeO_3 , $[H_{\text{STHF}}(\text{Cd}) / H(\text{Fe})] = 0.26 \pm 0.01$. We see that the ratios differ by approximately a factor of 2; the ratio for SR is the lower. To compare the Ru-site STHF in SR to the corresponding Fe-site STHF in PrFeO_3 , we take

two-fifths of $H_{\text{STHF}}(\text{Cd})=120$ kOe (based on $t_r=0.52$),¹⁷ which gives 48 kOe. The corresponding PAC-measured quantity in SR is 39 ± 3 kOe. The scaled PrFeO_3 value is about 20% greater than the measured value for SR. To compare the Ru-site total MHF in SR to the corresponding Fe-site total MHF in PrFeO_3 , we take two-fifths of $H(\text{Fe})=463$ kOe, which gives 185 kOe. The ME-measured quantity in SR is 315 ± 15 kOe. The scaled PrFeO_3 value is about 40% lower than the measured value for SR. Hence, the ratio $[H_{\text{STHF}}(\text{Cd})/H(\text{Ru})]=0.12$ for SR does not scale, because $H_{\text{STHF}}(\text{Cd})$ is somewhat smaller and $H(\text{Ru})$ is significantly larger than the corresponding scaled PrFeO_3 values. [We estimate that choosing a different REO model system such as either LaFeO_3 or NdFeO_3 would change the ratio $H_{\text{STHF}}(\text{Cd})/H(\text{Fe})$ by less than 10%.] A possible explanation is that conduction electrons and the associated itinerant exchange depletes the transfer of spin density through $^{111}\text{Cd-O-Ru}$ bonds and enhances the total MHF via conduction-electron polarization.²⁶

These results are interesting and unexpected. The measured total MHF at the Ru site in SR is almost twice as large as we would expect by considering the Fe-site total MHF in PrFeO_3 . However, all of the aforementioned measurements of the macroscopic magnetization^{2,3} indicate that M_s is smaller than $2\mu_B$, which is the value of M_s expected for a spin-only (low-spin) d^4 electron configuration. Presumably, delocalization of some of the Ru d electrons causes M_s to be less than $2\mu_B$. Unlike the results of the macroscopic magnetization, the total MHF measurements on SR, when they are compared to the reference crystal PrFeO_3 , indicate that the total MHF is enhanced. This result suggests that the delocalized $5s$ conduction electrons and perhaps some of the $4d$ conduction electrons may be more effective in polarizing the Ru nucleus than if these electrons were localized in $5s$ and $4d$ atomic orbitals. In comparison to the reference crystal, the Ru-site STHF is diminished in magnitude by a relatively small amount. This reduction could indicate that the delocalization of Ru d electrons also causes less spin

density to be transferred to ^{111}Cd $4s$ and $5s$ orbits through $^{111}\text{Cd-O-Ru}$ bonds.

V. CONCLUSIONS

Using the $^{111}\text{In}\rightarrow^{111}\text{Cd}$ PAC probe, we have measured nuclear-electric-quadrupole interactions at elevated temperatures at the Ru site in SR and very likely at the Ru site in CR. We also have measured combined nuclear magnetic-dipole and nuclear electric-quadrupole interactions at 77 K in SR. In SR, the temperature dependence of V_{zz} from 290 to 800 K indicates that SR undergoes a structural phase transition at ≈ 800 K that is similar in character to the tetragonal-to-cubic transitions that the ferroelectric perovskites BaTiO_3 and KNbO_3 undergo. This result implies that the laboratory-temperature crystal structure of SR has lower-than-cubic symmetry. At temperatures below this transition, the EFG asymmetry $\eta\approx 0.5$ associated with the Ru site in SR is too large to be attributed to the reported slight orthorhombic distortion. The CR crystal structure is much more distorted than the SR structure, and this distortion persists up to ≈ 1000 K. Then, as the temperature increases, the crystal becomes less distorted; and, as the temperature dependences of V_{zz} and η indicate, the CR crystal structure approaches the SR structure at temperatures above 1700 K. This transformation of the CR structure can be explained by the reduction in the tilting of O-octahedra as the temperature increases. At 77-K, at the Ru site in SR, the ratio of the STHF to the total MHF is approximately 0.12. Whereas the corresponding ratio in the model compound PrFeO_3 is about twice as large. This difference could result because the STHF is reduced by Ru-electron delocalization and the total MHF is enhanced by conduction-electron polarization.

ACKNOWLEDGMENT

We gratefully acknowledge support for this project for the Office of Naval Research (Grant No. N00014-90-J-4112).

¹J. J. Randall and R. Ward, *J. Am. Chem. Soc.* **81**, 2629 (1959).

²A. Callaghan, C. W. Moeller, and R. Ward, *Inorg. Chem.* **5**, 1572 (1966).

³J. M. Longo, P. M. Raccach, and J. B. Goodenough, *J. Appl. Phys.* **39**, 1327 (1968).

⁴R. J. Bouchard and J. L. Gillson, *Mater. Res. Bull.* **7**, 873 (1972).

⁵V. I. Spitsyn, I. M. Kulshov, N. A. Shishakov, and N. F. Shakhova, *Russian J. Inorg. Chem.* **18**, 592 (1973).

⁶C. N. R. Rao, P. Ganguly, K. K. Singh, and R. A. Mohan Ram, *J. Solid State Chem.* **72**, 14 (1988).

⁷W. Bensch, H. W. Schmalle, and A. Reller, *Solid State Ion.* **43**, 171 (1990).

⁸C. B. Eom, R. J. Cava, R. M. Fleming, J. M. Phillips, R. B. van Dover, J. H. Marshall, J. W. P. Hsu, J. J. Krajewski, and W. F. Peck, Jr., *Science* **258**, 1766 (1992).

⁹K. Char, M. S. Colclough, T. H. Geballe, and K. E. Myers, *Appl. Phys. Lett.* **62**, 196 (1993).

¹⁰X. D. Wu, S. R. Foltyn, R. C. Dye, Y. Couleter, and R. E. Muenchausen, *Appl. Phys. Lett.* **62**, 2434 (1993).

¹¹F. Lichtenberg, A. Catana, J. Mannhart, and D. G. Schlom, *Appl. Phys. Lett.* **60**, 1138 (1992).

¹²J. Mannhart, J. G. Bednorz, K. A. Müller, D. G. Schlom, and J. Ströbel, *J. Alloys Compounds* **195**, 519 (1993).

¹³C. B. Eom, R. B. van Dover, J. M. Phillips, D. J. Werder, J. H. Marshall, C. H. Chen, R. J. Cava, and R. M. Fleming, *Appl. Phys. Lett.* **63**, 2570 (1993).

¹⁴T. C. Gibb, R. Greatrex, N. N. Greenwood, and P. Kaspi, *Chem. Commun.* **1971**, 319 (1971).

¹⁵T. C. Gibb, R. Greatrex, N. N. Greenwood, and P. Kaspi, *J. Chem. Soc. Dalton Trans.* **1973**, 1253 (1973).

¹⁶See, for example, M. Marezio, J. P. Remeika, and P. D. Dernier, *Acta Crystallogr. Sec. B* **26**, 2008 (1970).

¹⁷T. M. Rearick, G. L. Catchen, and J. M. Adams, *Phys. Rev. B* **48**, 224 (1993).

¹⁸G. L. Catchen, S. J. Wukitch, E. M. Saylor, W. Huebner, and

- M. Blazkiewicz, *Ferroelectrics* **117**, 175 (1991).
- ¹⁹J. M. Adams and G. L. Catchen, *Mater. Sci. Eng.* **B15**, 209 (1992).
- ²⁰G. L. Catchen, E. F. Hollinger, J. M. Adams, and R. L. Raseria, *Ferroelectrics* (to be published).
- ²¹G. L. Catchen, *J. Mater. Educ.* **12**, 253 (1991).
- ²²G. L. Catchen, J. M. Adams, and T. M. Rearick, *Phys. Rev. B* **45**, 5015 (1992).
- ²³For a theoretical description of this effect, see G. L. Catchen, *Hyperfine Interact.* (to be published).
- ²⁴D. Treves, *J. Appl. Phys.* **40**, 1061 (1969).
- ²⁵M. Eibschütz, S. Shtrikman, and D. Treves, *Phys. Rev.* **156**, 562 (1967).
- ²⁶For a discussion of conduction-electron polarization and core polarization, see D. A. Shirley, S. S. Rosenblum, and E. Matthias, *Phys. Rev.* **170**, 363 (1968).